Atmos. Chem. Phys. Discuss., 8, 4625–4667, 2008
www.atmos-chem-phys-discuss.net/8/4625/2008/

Atmospheric Chemistry and Physics Discussions

Simulation of dust aerosol and its regional feedbacks over East Asia using a regional climate model

D. F. Zhang[1], **A. S. Zakey**[2], **X. J. Gao**[1,2], **and F. Giorgi**[2]

[1]The Laboratory of Climate Study of China Meteorological Administration, National Climate Center, 100081, Beijing, China
[2]Abdus Salam International Centre for Theoretical Physics, 34100, Trieste, Italy

Received: 11 December 2007 – Accepted: 9 January 2008 – Published: 4 March 2008

Correspondence to: A. S. Zakey (azakey@ictp.it)

Published by Copernicus Publications on behalf of the European Geosciences Union.

Abstract

The ICTP regional climate model (RegCM3) coupled with a desert dust model is used to simulate the radiative forcing and related climate effects of dust aerosols over East Asia. Two sets of experiments encompassing the main dust producing months, February to May, for 10 years (1997–2006) are conducted and inter-compared, one without (Exp. 1) and one with (Exp. 2) the radiative effects of dust aerosols. The simulation results are evaluated against ground station and satellite data. The model captures the basic observed climatology over the area of interest. The spatial and temporal variations of near surface concentration, mass load, and emission of dust aerosols from the main source regions are reproduced by model, with the main model deficiency being an overestimate of dust amount over the source regions and underestimate downwind of these source areas. Both the top-of-the-atmosphere (TOA) and surface radiative fluxes are decreased by dust and this causes a surface cooling locally up to −1°C. The inclusion of dust radiative forcing leads to a reduction of dust emission in the East Asia source regions, which is mainly caused by an increase in local stability and a corresponding decrease in dust lifting. Our results indicate that dust effects should be included in the assessment of climate change over East Asia.

1 Introduction

Atmospheric aerosols are still considered one of the main sources of uncertainty within the climate change debate (IPCC, 2007). In particular, increasing attention is being paid to the effect of desert dust, since dust clouds can affect long- and short-wave radiation and can play an important role in modifying climate at the regional scale (Christopher et al., 2003; Dey et al., 2004). In this regard, it is worth mentioning that no AOGCM used for climate change projections in the IPCC fourth assessment report includes the effects of desert dust.

Dust aerosol affects the atmosphere's radiation budget (Tegen et al., 1996; Sokolik

ACPD

8, 4625–4667, 2008

et al., 1996) and chemical composition (Dentener et al., 1996; Dickerson et al., 1997; Martin et al., 2003). The broader impacts of the dust cycle have been investigated in studies of Chinese loess/paleoclimate relationships (Zhang, 1984; Porter, 2001) and in the observations of Asian dust storm frequencies made during the last century (Natsagdorj et al., 2003; Zhang et al., 2003a, b). The former provide some perspective on the dust–climate interactions that operated before the Earth system became perturbed by human activities.

Due to the uncertainties in the estimates of dust loadings and radiative properties of dust aerosols, it is difficult to estimate the dust radiative effects (Sokolik et al., 1996; Myhre et al., 2001; Aoki et al., 2005). On the global scale, estimates of dust emissions differ by more than a factor of two (ranging from 1000 to 2150 $\mathrm{Tg\,yr^{-1}}$), while the dust mass load estimates range by a factor of four (8–36 $\mathrm{Tg\,yr^{-1}}$) (Zender et al., 2004). Since the late 1980s, models for global, regional and local dust simulation have been developed. Early attempts of dust modeling were made by Westphal et al. (1988), Gillette et al. (1989), and Joussaume (1990). Examples of global dust models include the studies of Tegen et al. (1994), Ginoux et al. (2004), Zender et al. (2003) and Tanaka et al. (2003). Examples of regional studies include Shao et al. (1997), Nickovic et al. (2001), Gong et al. (2003), Liu et al. (2003), and Zakey et al. (2006), while regional climatologic characteristics of dust phenomena have been described in some observational studies (Pye, 1987; Goudie et al., 1992).

East Asia is one of the most prominent regions of dust generation. Asian dust source regions include the Gobi desert and the highlands of northwestern China (Zhang et al., 2003a). Over East Asia, estimation of dust aerosols is particularly difficult due to complex topography, land-use, and snow cover features. In fact, dust concentrations over East Asia tend to be systematically underestimated by global models (Tegen et al., 2002; Luo et al., 2003).

Observational evidence suggests that dust originating from East Asia has a significant influence even at the global scale. For example, it is reported that East Asian dust can be transported to wide areas of the Pacific Ocean (Husar et al., 2001), reaching

ACPD
8, 4625–4667, 2008

as far as North America (McKendry et al., 2001) during severe dust storm events. Deposits of Asian dust have been identified from snow samples in Greenland (Biscaye et al., 1997; Bory et al., 2003) and even in the French Alps (Grousset et al., 2003). Dust storms over East Asia occur primarily in spring, when strong winds entrain large quantities of dust particles into the atmosphere and carry them downstream (Zhang, 2001; Shao et al., 2006). Extremely severe dust storms in the past have resulted in the loss of human lives and the disruption of economic activities (Cheng et al., 1996). In fact, dust storms are widely recognized as a serious environmental problem in East Asia and have attracted much scientific attention. In China, arid and semiarid areas occupy 3.57 million km^2 (Shao et al., 2006). The desert distribution from west to east is shown in Table 1. These deserts, as well as the Gobi in Mongolia, are the main sources of East Asia dust storms (Qin et al., 2002).

The climatology of dust storms in China is quite well documented through the analysis of synoptic records over the past 50 years (Zhou, 2001; Chun et al., 2001; Kurosaki et al., 2003; Shao et al., 2003) and of satellite data in more recent years (Prospero et al., 2002). The number of dust storm occurrences during the period 1954–2002 shows that, with respect to the annual total, the percentage of the occurrence of strong dust episodes is 6.3% in February, 18.4% in March, 44.4% in April, and 19.7% in May (Zhou et al., 2003). A decreasing trend of strong dust storm occurrence has been observed in recent decades. The maximum storm occurrence is found in the 1950s, followed by a continuous decrease until the 1990s and a slight increase since 2000 (Zhou et al., 2003). According to synoptic records over the past 50 years, 2000, 2001 and 2002 are among the most active years in terms of severe dust storm occurrence over East Asia (Zhang et al., 2002). Because wind speed plays the main role in dust initiation, the correlation coefficient of wind with the number of dust storm occurrence exceeds 50% at the stations studied. A decrease of dust storm occurrence can thus be the result of decreasing wind speed following a change of the general atmospheric circulation (Zhou et al., 2001).

From these considerations it is clear that desert dust is a major element of the en-

ACPD
8, 4625–4667, 2008

vironment of East Asia, and might thus be an important component of climate change over the region. In order to study the effects of dust on regional climate, Zakey et al. (2006) developed a radiatively active desert dust module and coupled it to a regional climate model (the ICTP RegCM3) (Pal et al., 2007). We here use this coupled modeling system to provide a preliminary study of the potential dust effects on the climate of East Asia. It is noted that former simulations on dust storms over the region mostly focused on individual case studies in which the dust was not radiatively coupled with the meteorological models (Zhang et al., 2003a, b; Zhao et al., 2006b). Therefore, this is the first long term simulation of dust radiative effects over East Asia.

The primary purpose of the present study is to present a first evaluation of our modeling system over this region, going from dust emission and burden to dust radiative effects and regional climatic response. In this regard, two important caveats should be highlighted: 1) We do not include long-wave effects of the dust aerosols; and 2) we do not include the interaction of dust with the cloud microphysics. Development of parameterizations of these processes is currently under way and their implementation and testing within our modeling system is left to future work.

In Sect. 2 we first describe the model and experiment design, while in Sect. 3 we discuss the model results for the area of study. In particular, we analyze surface emission, near surface concentrations, dry and wet deposition processes, aerosol optical properties, and radiative forcing. Our concluding considerations and perspectives for future work are presented in Sect. 4.

2 Model, data and experiment design

The model employed in the present study is the Regional Climate Model RegCM version 3 (RegCM3) developed at the Abdus Salam International Centre for Theoretical Physics (ICTP) (Pal et al., 2007). RegCM3 is an evolution from the version of Giorgi et al. (1993a, b), with improvements in various physics packages (Pal et al., 2007). Atmospheric radiative transfer processes are from the NCAR global model CCM3, which

ACPD
8, 4625–4667, 2008

are described by Kiehl et al. (1996). Land surface processes are represented via the Biosphere-Atmosphere Transfer Scheme (BATS1e; Dickinson et al., 1993), while planetary boundary layer computations employ a non-local formulation (Holtslag et al., 1990). The mass flux scheme of Grell (1993) is used to describe convective precipitation and the Sub-grid Explicit Moisture Scheme of Pal et al. (2000) is used to describe non-convective precipitation.

For dust calculations we use the dust module developed and implemented by Zakey et al. (2006). Transport processes are described by the tracer transport equation of Solmon et al. (2006), which includes advection by resolvable scale winds, transport by turbulence and deep convection, gravitational settling, wet and dry removal processes. Wet deposition is treated following Giorgi (1989) for large-scale precipitation and Giorgi et al. (1986) for convective precipitation. The gravitational settling and dry deposition terms are described by Zakey et al. (2006).

The dust production scheme is based on Marticorena et al. (1995) and Alfaro et al. (2001) and essentially comprises three key components (Zakey et al., 2006): Eq. (1) the threshold friction velocity at which wind erosion is initiated, Eq. (2) the horizontal and vertical dust emission flux and Eq. (3) the surface and soil-related factors influencing either the threshold friction velocity or the dust fluxes (e.g. soil water content and soil texture type). Coagulation of dust aerosols and interactions with clouds are currently not represented. The whole size range of the dust aerosols (0.01–20 μm) is divided into four size bins (0.01–1.0 μm), (1.0–2.5 μm), (2.5–5.0 μm) and (5.0–20 μm) and the evolution of each size bin is represented by a prognostic equation written for the dry size of the particle (Zakey et al., 2006).

In our simulation the following data sets are used: 1) Meteorological initial and time-evolving lateral boundary conditions for the RegCM simulations are from the National Center for Environmental Prediction/National Center for Atmospheric Research (NECP) re-analysis (Kalnay et al., 1996); 2) Land use types are based on observed data within China (Hou, 1982) and satellite GLCC data developed by the USGS outside China (Loveland et al., 2000); 3) Soil texture data sets are based on USDA texture

ACPD
8, 4625–4667, 2008

classification (USDA, 1999) with some modifications in central and northeast China for extra dust sources (Tengger, Onqin Daga, and Horqin) following Zhao et al. (2006b).

The model domain encompasses the whole continental China and adjacent areas (see Fig. 1) at a horizontal grid spacing of 50 km. It includes the primary dust regions in China. The model is run at its standard configuration of 18 vertical sigma layers and model top at 100 hPa. Within the domain we identify three regions for more specific analysis (Fig. 1): 1) West (35.5°–44° N, 75°–95° E), 2) Central (33°–44° N, 95°–112° E), and 3) East (30°–46° N, 112°–130° E). Observed data from nine stations are used for the validation of the dust module (Fig. 1).

Each model simulation extends from 1 November to 1 June of the following year. In this way the model can generate its seasonality of snow cover before our analysis period, which is February-March-April-May (FMAM), when most dust storms occur over the region. We simulated 10 years, from 1997 to 2006 and for each of these year two sets of experiments are conducted. The first (Exp. 1) includes the dust model, but the dust is not radiatively active, i.e. the dust climate feedback is not accounted for. In the second set (Exp. 2), all the conditions are the same as in Exp. 1, but the dust is radiatively interactive, which allows us to capture dust-climate feedbacks.

The radiative code in the RegCM employs the δ-Eddington approximation for radiation flux calculations, and the wavelength spectrum is divided into 18 discrete intervals from 0.2 to 4.5 μm. Seven of these span the ultraviolet (0.2 to 0.35 μm), and one covers the visible (0.35 to 0.7 μm). In our aerosol forcing calculations we use these eight wavelength bands and in order to reduce the computational cost we only calculate parameters for mid-band (0.35–0.7 μm) wavelength. The dust direct radiative forcing is described in terms of three optical parameters, the asymmetry factor, the single scattering albedo, and the specific extinction coefficient. The values of these dust optical parameters for different wavelengths and particle size are obtained from Mie calculation. The refractive indices of mineral dust (real and imaginary parts) for each wavelength (0.25–40 μm) are taken from the recent work of Balkanski et al. (2007) and from OPAC database (Hess et al., 1998).

ACPD
8, 4625–4667, 2008

In order to calculate the dust radiative forcing we compute the dust aerosol optical depth (AOD) and dust index (DI) within the RegCM as described in Zakey et al. (2006). The general relationship between the dust extinction optical depth "τ" and its mass loading per unit area "M" can be expressed as:

$$\tau = \frac{3QM}{4\rho r_e} \quad (1)$$

where ρ is the dust particle density, r_e is the effective radius, and Q is the extinction coefficient, which is calculated from Mie theory. Both τ and Q are wavelength-dependent. The most convenient way of linking the dust optical depth with its dry mass "m_d" is $\tau=\beta m_d$, where β is the specific extinction or mass extinction efficiency (m^2g^{-1}), defined as,

$$\beta = \frac{3QM}{4\rho r_e m_d} \quad (2)$$

The dust index for 550 nm is then calculated as (Ginoux et al., 2003):

$$DI = (1 - 0.2\log(P_s))\left[1.25 + 5\,(1 - \omega_{550})\,h\right](\tau_{550})^{\omega_{550}} \quad (3)$$

where P_S is the surface pressure, ω_{550} is the single scattering albedo, τ_{550} is the optical depth at 550 nm, h is the depth of the aerosol layer (scale height of dust particles, in km). We use the 550 nm wavelength because this is the most effective wavelength in the short wave spectrum and in order to compare with the MISR satellite data (see below).

3 Results and discussion

3.1 Climatic feature of the region

Simulation and basic understanding of the regional climatology of East Asia are important for the evaluation of dust-induced climate feedbacks. The climate of East Asia

shows marked seasonality. Winter climate is characterized by dry and cold conditions caused by the mid-latitude westerly jet, which sweeps across the region from the continental interior carrying predominant dry and cold air. The summer season is dominated by the onset and development of the East Asia monsoon. As a result of the northward and westward evolution of the western subtropical Pacific High, moist southwesterly monsoon flow dominates over the region, inducing warm and wet conditions. Spring, our season of interest, is a transition period between these two climate regimes.

Mean geopotential height and wind fields for FMAM at 850 hPa from the NCEP re-analysis and model simulation are shown in Figs. 2a and 2b, respectively. A deep trough (the East Asia Trough) over the northeastern coastal region can be found in the re-analysis data (Fig. 2a). This brings cold and dry continental air from high latitudes to north and northeast China. Conversely, southeast China is dominated by southerly winds and it is affected by sub-tropical systems occurring in correspondence of the pre-onset stage of the monsoon. The model simulates the East Asia Trough, although this appears to be somewhat deeper than in the re-analysis and leads to an overestimate of northwesterly winds over north and northeast China (Fig. 2b).

Figure 2c shows FMAM observed precipitation from the Climate Research Unit, (CRU) of the University of East Anglia (Mitchell et al., 2005) averaged over the period 1997–2002 (later years were not available). This precipitation is characterized by maxima over southeast China and a decrease towards the north and northwest. Less than 0.5 mm day^{-1} precipitation is found over northwest China, which is an arid and semi-arid area where the main sources of dust production are located. The model reproduces this basic precipitation pattern (Fig. 2d), however, a general overestimate of precipitation is found over north and northwestern China and an underestimate over southeast China. The largest overestimate can be found in areas of complex topography, e.g. over the eastern edge of the Tibetan Plateau (near 112° E, 32° N). However this may be related to insufficient observations and no gauge under catch and topographical corrections of the data.

The simulated surface air temperature shows a generally good agreement with ob-

ACPD
8, 4625–4667, 2008

servations as shown in Figs. 2e and 2f, with a cold bias of a few °C or less over central and south China. The model also shows a slight warm bias over northeast China. Overall, the model shows a performance in line with that found in previous analysis-driven simulations over this region (Zhang et al., 2007).

3.2 Dust concentration, mass load, emission and removal

The simulated annual average near surface dust concentration at the lowest model level is compared with the Air Quality Index (AQI) over China for the period 2001–2006 (available data) in Fig. 3. The AQI is a function of PM_{10}. Although it also includes other particulate matter sources, it is still a good indicator of relative inter-annual variations in dust concentration (Gong et al., 2003). AQI data from nine stations across China are selected for comparison with the closest model grid point (see Fig. 1 and Table 2). The simulated near-surface concentration ($\mu g\,m^{-3}$) and observed AQI (unit-less) in Fig. 3 are based on two separate vertical axes with different scales because of the different units (Gong et al., 2003). This comparison is therefore not intended to be quantitative but to indicate whether the model captures the general inter-annual variation of near surface concentration at the selected stations. For this measure, the model shows a reasonably good performance at most stations, except Ulmuqi which is close to the main area of dust source (Taklimakan and Gurbantunggut). This may be due to the complex geographic location of the station. Ulmuqi is located in a narrow valley at the foothills of the high mountains, facing the Junggar Basin. However, the model resolution (50 km) is not fine enough to capture the real height of this station. In particular the model grid point lies at a higher elevation and therefore it might be characterized by more dilution and higher variability in the near surface concentration.

The inter-annual variation of dust mass load, dust emission, wet and dry deposition, surface wind speed, and precipitation over the three regions of Fig. 1 are shown in Fig. 4. A lower emission, mass load, wet and dry depositions are found in the East region compared to the West and Central regions. This is because the East region has the smallest dust sources, and the dust mass load there is mostly derived by transport

ACPD
8, 4625–4667, 2008

from upwind larger source areas. Conversely, while the largest emission and mass loads are found in the Central region. In general a good correlation is found between the inter-annual variations of mass load, emission, and removal (wet and dry) at the three regions. This for two reasons: first, dust sources affect both the region they are in and the downwind regions; second, dust producing circulations occur at the broad regional scale and tend to affect both the West and Central main dust source regions.

A further measure of dust dispersion is the ventilation index (VI) (Hsu, 2003; Rao, 2003), which is defined as the product of boundary-layer height and a representative boundary-layer horizontal wind speed. Large values of these two factors imply pronounced vertical and horizontal dust lifting and dispersion. Figure 5 compares the annual average VI and dust concentrations at the 9 selected station sites, showing that variations of VI show similarities to the dust concentrations at these sites. The results indicate that higher VI generally leads to a higher dust concentration in the atmospheric boundary layer, with the exception of 1998. A severe dust storm occurred in April of this year leading to 2–4 times higher near surface dust concentration than any other dust event since 1988 (Husar et al., 2001) and this substantially contributed to the 1998 dust maximum.

3.3 Optical properties of dust particles

In our simulation the optical properties of dust particles are calculated for each size bin at each spectral band of the radiation package (which includes 18 spectral bands). As mentioned, in order to save computation time and to compare with the MISR data, only the band of 350–640 nm centered at 550 nm is used in the model to compare with satellite measurements. Correspondingly, the radiative forcing is calculated for the same band.

ACPD
8, 4625–4667, 2008

3.3.1 Dust aerosol optical depth (AOD)

Multi-angle Imaging Spectro-radiometer (MISR, 550 nm) satellite (2001–2006, available data) and multi-year monthly mean AOD from the model (1997–2006) are shown in Fig. 6. The comparison shows that the model captures the areas of maximum dust optical depth; however the peak AOD values are higher than obtained from the MISR estimates, particularly over the Central source region. Compared to the MISR data, the model tends to produce excessively large dust amounts over the source areas and lower amounts away from these regions. This is an indication of relatively weak long range dispersal of the dust plume. Most of this dispersal occurs by lifting and detrainment above the boundary layer and subsequent transport by free tropospheric winds.

To illustrate this process, Fig. 7 shows a longitude-vertical cross section of dust amount for the latitude band 38–42° N, which encompasses the main dust source areas, averaged for the 10 simulated years. Although some dust is transported all the way into the Pacific Ocean (up to 150° E), it is evident that most of the dust amounts are confined within the atmospheric boundary layer, below about 800 hPa. Significant dust amounts reach the mid troposphere (about 500 hPa) but no substantial dust amounts reach the upper troposphere, where it would be transported more effectively by the upper tropospheric winds. It is interesting to notice that a similar problem was not found by the application of this dust module to the Sahel/Sahara region (Zakey et al., 2006). In this latter case, most of the vertical transport was achieved through vigorous cumulus convection occurring in the summer time. In the spring season over East and North Asia, convection is not strong and contributes less to vertical transport, which is more related to meso and synoptic scale processes which are evidently under-represented by the model. A better understanding of this issue requires vertical dust profile data, which is currently not available. However we plan a more detailed investigation of the structure of individual dust storms in future work. We finally note that the intra-seasonal variation of the maximum AOD at these source areas is well captured by model, with the dust production increasing from February to April and then starting to decrease in

ACPD
8, 4625–4667, 2008

May (see Fig. 6).

Over eastern China the retrieved AOD from satellite is substantially higher than simulated by the model. However, a large (and perhaps dominant) contribution to this overestimate is given by the fact that the MISR AOD detects all types of aerosols, including sulfate, black carbon, and organic carbon of anthropogenic origin (Zhao et al., 2006a; Giorgi et al., 2002), which are not included in the current simulations. Note for example the very large AOD (in excess of 0.6) over the Sichuan basin in southwest China and the Shanghai area in the eastern coastal regions, which is due to intense industrial activities there. In fact, the optical properties of dust depend on the particle size and refractive index. Uncertainties in these properties could lead to large uncertainties in direct radiative forcing (Sokolik et al., 2001) and this could also contribute to our underestimated values.

There are very limited numbers of continuous AOD observations from AERONET sun photometer stations in East Asia. For this reason, for model validation we selected only one site at Dalanzadgad (43.6° N, 104.4° E), where the desert dust aerosol can be considered to be dominant (Fig. 8). This comparison shows that the simulated AOD is generally in line with observations. The correlation coefficient between the simulated and observed AOD for this AERONET station is 0.55 for the period from March 1998 to March 2004 (available data), which is significant at the 99% confidence level.

3.3.2 Comparison of the simulated dust index (DI) with the aerosol index (AI) from satellite observations

As mentioned above, we calculate the dust index (DI) following Ginoux et al. (2003). We then compare the DI with monthly mean AI from the Total Ozone Mapping Spectrometer (TOMS, 380 nm, 1997–2005), Ozone Monitoring Instrument (OMI, 2006) data sets. Averaged DI and AI for the period 1997–2006 are shown in Fig. 9. The results from this comparison are in line with what found when comparing with the MISR data. The spatial distribution patterns of DI show a good agreement over the two main areas of dust production, although the model overestimates the peak DI values at the Central

region. Conversely, the DI is underestimated away from the source areas. Although this can be partly attributed to the absence of background aerosols in the model, it is again an indication of weak simulated dispersal (see discussion above). We also note that the intra-seasonal variation of the AI, with the maximum in April and minimum in February is well captured by the model.

Figure 10 shows the daily AI and DI in the selected regions from February to May for the years 1998 and 2001, i.e. two years when a relatively high number of dust events occurred. The results show that the model captures the occurrence of the main individual dust events, although the magnitude of the event may be different from observed. The correlation coefficients between the daily AI from satellites and the DI from the simulations for each year are presented in Table 3. The mean values of the correlation coefficients are 0.35, 0.27 and 0.41, for the West, East and Central regions, respectively, and are all statistically significant at the 99% confidence level. In the West region, 8 out of the 10 years show significant correlation, while in the Central and East regions, this is found in 4 and 9 out of the 10 years (Table 3).

Figure 10 also shows that, while the model captures the occurrence of individual events, sometimes even producing larger values of DI than observed, it underestimates the observed values during the periods that separate the events and more generally it underestimates the amount of background aerosol. This problem is evidently related to the relatively weak simulated dust dispersion discussed above.

Direct observations of dust storms reported by meteorological stations and synoptic reports have been widely used to establish the climatology of dust emissions in arid and semiarid regions. In northeastern Asia, Goudie (1983) identified the Taklimakan desert as the most frequent source of dust storms, with 33 dust storms per year, and the northern desert of China as the second source with a maximum of 19 dust storms in the Badain Jaran desert. Here we use three different emission thresholds to identify the occurrence of a dust event simulated by the model: 5000, 10 000 and 15 000 mg m^{-2} day^{-1}. Results of dust occurrence related to these three thresholds are shown in Fig. 11 and Table 4.

ACPD
8, 4625–4667, 2008

According to our emission thresholds, the model shows that April is the most frequent in the West and East regions and March is the most frequent in the Central region (Table 4). In March the Central region shows the highest frequency of dust storms, with percentages of 31, 34 and 48% for the 5000, 10 000 and 15 000 mg m^{-2} day^{-1} thresholds, respectively. Zhou et al. (2003) found that the frequency of most severe dust storms peaks in the Tarim Basin, the eastern part of the Northwest China and North China, which is consistent with our results.

Figure 11 shows the total number of dust storm occurrence for each year, region and threshold. When looking at the smallest threshold the West region emerges with the largest number of storms, in particular with maxima in 1998, 2002 and 2004. At the higher thresholds the Central region becomes the most frequent dust source, with marked maxima in 2001 and 2004. The lowest threshold number of occurrence varies from about 32–49 in the West region and the highest one varies from about 1–19 in the Central region. East region shows only a small number of dust source occurrences.

3.4 Dust feedback on regional climate

As mentioned, dust, as one of the major natural aerosol in East Asia, can influence the climate of the region by altering the radiative budget of the surface and atmosphere. Dust scatters and partly absorbs incoming solar radiation, and it also absorbs and re-emits outgoing long-wave radiation. Any changes in atmospheric dust loads would cause changes in the radiation balance and, consequently, would affect surface temperatures and other climatic variables. The magnitude and even the sign of the direct radiative dust forcing is uncertain, since it depends on the optical properties of the dust, its vertical distribution, cloud cover, and the albedo of the underlying surface (Liao et al., 1998). The top-of-atmosphere (TOA) forcing due to dust is believed to be small when globally averaged due to the cancellation of regionally positive and negative forcing depending on the underlying albedo. Conversely the reduction of surface radiation by dust is significant even at the global scale, and it has been estimated at 1–2 W m^{-2} (Tegen et al., 1996; Woodward et al., 2001).

As mentioned, in our model we only include short wave absorption and reflection by dust, with the latter providing the dominant contribution (Shell et al., 2007). Therefore, we expect a dominant negative radiative forcing of dust. Figure 12a presents the multi-year average TOA dust radiative forcing and indeed it shows that this is mostly negative and in the range of -2.5 to $-10\,W\,m^{-2}$. The maximum negative radiative forcing is over the western dust source region.

Figure 12b shows the surface dust radiative forcing. This is negative everywhere and reaches relatively high values, up to $-25\,W\,m^{-2}$. Again, the maximum negative surface radiative forcing is found over the West and Central dust source regions. Atmospheric heating rates are increased and long-wave surface cooling rates are decreased by the presence of dust, as shown in Fig. 12c–d. Both downward and net long-wave radiation at the surface are decreased by $-2\,W\,m^{-2}$ and $-4\,W\,m^{-2}$, respectively (Fig. 12e–f), essentially as a result of surface cooling. The negative surface radiative forcing due to short wave reflection in fact causes a pronounced cooling over the major dust source areas, with values in the range of -0.5 to $-1^{\circ}C$ (Fig. 12g). The cooling in areas downwind of the source regions is less pronounced, but still of the order of -0.1 to $-0.5^{\circ}C$.

Figure 12h shows the multi-year mean difference in dust mass load between Exp. 2 (with dust feedbacks) and Exp. 1 (without dust feedbacks). This shows a reduction of dust mass of several hundreds mg m^{-2} over the source regions and 10 to 250 mg m^{-2} over the downwind regions. This result is consistent with those of (Perlwitz et al., 2001), who found that dust feedbacks lead to a reduction of about 10% in dust mass load.

To elucidate the mechanisms underlying this feedback, Figs. 13a–f show the change of annual averaged mass load, emission, removal, surface air temperature, wind speed and precipitation respectively, over the three source regions. A decrease of mass load is found over all the three regions, with the greatest decrease in the Central (Fig. 13a). This decrease in dust load is clearly associated with a decrease in emissions over all regions (Fig. 13b), which in turn is mostly related to the stabilization of the lower boundary layer by the surface cooling and thus the reduction of dust mobilization and lifting (as measured in the dust parameterization by the friction velocity). Changes in

ACPD
8, 4625–4667, 2008

large scale circulations do not appear to be a factor as indicated by the fact that Fig. 13e does not show significant changes in wind speed.

Dust removal also decreases over all regions (Fig. 13c), mostly because of decreased dust amounts, since the dust feedbacks do not produce a large systematic effect on precipitation (only a small decrease, Fig. 13f). The average surface air temperature decreases by 0.30–0.56°C, 0.18–0.42°C, 0.06–0.19°C over the West, Central and East regions, respectively (Fig. 13d). Note that these values are comparable to (and locally higher than) the greenhouse gas induced warming observed in the latest decades of the 20th century (IPCC, 2007).

In summary, the dust feedbacks induces a negative TOA and surface radiative forcing, which in turn causes surface cooling, a decrease of dust mobilization over the source areas and a reduction of mass load.

4 Summary and conclusions

In this paper we use a coupled regional climate-dust model (the ICTP RegCM3) to simulate desert dust production and regional climatic effects over East Asia. We analyze the simulation of ten spring seasons (i.e. the season of maximum dust production over the region) and evaluate the model performance against available observations, both ground based and from satellite. Finally, we assess the radiative forcing and feedbacks of the dust aerosols over the region.

The results show that the model reproduces the basic climatology over the region and that the dust model performs reasonably well in simulating the spatial distribution, intra-seasonal variation and multi-year mean monthly variation of near surface concentration, AOD, and DI. The primary model deficiency is an overestimate of dust load and AOD over the source regions and a corresponding underestimate away from these regions. This problem is symptomatic of relatively weak lifting of dust into the free troposphere and weak dispersal. In future work we plan to investigate in more detail the dynamical mechanisms that lead to this problem and improve the model performance

ACPD
8, 4625–4667, 2008

in this respect.

The dust exerts a substantial negative TOA and surface radiative forcing, leading to surface cooling of several tenths of ˚C to 1˚C over the source regions and downwind areas. The surface cooling causes a decrease of dust load because of increased stability and reduced dust mobilization. As a result, the dust radiative forcing produces a negative feedback mechanism. The effects of dust on regional temperatures are locally comparable to those expected from increases of greenhouse gas concentrations, which suggest that dust should be included in climate change studies over this region.

Our study is limited in three aspects. Firstly, we do not include the contribution of other aerosols, e.g. sulfate, black carbon and organic carbon, which have been proven to be important over East Asia (Giorgi et al., 2002). This is because in this study we wanted to isolate the effects of dust. However, our modeling system has the capability of including such additional aerosols (Solmon et al., 2006), so that we plan to perform new sets of simulations including all aerosol types. Secondly, indirect effects, e.g. the role of dust particles as cloud condensation nuclei, are not described in our simulation and we are currently implementing in our model a new cloud microphysics and indirect effect scheme. Third, our simulation does not take into account the long-wave emissivity of dust, which tends to counterbalance the short-wave cooling effect over the dust source region. TOA long-wave forcing efficiency has been reported for example by Zhang and Christopher (2003) based on satellite measurements and by Haywood et al. (2005) based on theoretical considerations. Some modeling studies show positive net TOA forcing over the source region when long wave emissivity is accounted for (Balkanski et al., 2007; Miller et al., 2004). However, the recent study of Yoshioka et al. (2007) still finds a dominant negative TOA forcing even when taking into account the long wave spectrum. It thus appears that still substantial uncertainty is present on the estimates of the contribution of long-wave dust emissivity, and we are in the process of incorporating dust long-wave emissivity effects in our model to test the eventual modifications of the dynamical responses outlined in the present study.

Eventually we plan to use the full model with multiple aerosols, short and long wave

ACPD
8, 4625–4667, 2008

radiative forcing and direct and indirect effects to climate change simulations over East Asia.

Acknowledgements. This research is jointly supported by the National Key Program for Developing Basic Sciences (2006CB403700, 2006CB400506) of China and Climate Change Study Fund of the China Meteorological Administration.

References

Alfaro, S. C. and Gomes, L.: Modelling mineral aerosol production by wind erosion: Emission intensities and aerosol size distributions in source areas, J. Geophys. Res., 106, D16, 18 075–18 084, 2001.

Aoki, T., Tanaka, T. Y., Uchiyama, A., Chiba, M., Mikami, M., and Key, J. R.: Sensitivity experiments of direct radiative forcing by mineral dust using spectrally detailed radiative transfer model, J. Meteorol. Soc. Jpn., 83A, 315–331, 2005.

Balkanski, Y., Schulz, M., Claquin, T., and Guibert, S.: Reevaluation of mineral aerosol radiative forcings suggests a better agreement with satellite and AERONET data, Atmos. Chem. Phys., 7, 81–95, 2007, http://www.atmos-chem-phys.net/7/81/2007/.

Biscaye, P. E., Grousset, F. E., Revel, M., der Gaast, S. V., Zielinski, G. A., Vaars, A., and Kukla, G.: Asian provenance of glacial dust (stage 2) in the Greenland Ice Sheet Project 2 Ice Core, Summit, Greenland, J. Geophys. Res., 102, C12, 26 765–26 781, 1997.

Bory, A. J. M., Biscaye, P. E., and Grousset, F. E.: Two distinct seasonal Asian source regions for mineral dust deposited in Greenland (NorthGRIP), Geophys. Res. Lett., 30, 4, 1167, doi:10.1029/2002GL016446, 2003.

Cheng, L. S. and Ma, Y.: The developing structure of a black storm and its numerical experiment of different model resolution, Quarter J. Appl. Meteor., 7, 386–395, 1996 (in Chinese).

Christopher, S. A., Wang, J., Ji, Q., and Tsay, S.: Estimation of diurnal shortwave dust aerosol radiative forcing during PRIDE, J. Geophys. Res., 108, D19, 8596, doi:10.1029/2002JD002787, 2003.

Chun, Y. S., Boo, K. O., Kim, J., Park, S., and Lee, M.: Synopsis, transport and physical characteristics of Asian dust in Korea, J. Geophys. Res., 106, D16, 18 461–18 469, 2001.

Dentener, F. J., Carmichael, G. R., Zhang, Y., Lelieveld, J., and Crutzen, P. J.: Role of mineral

dust aerosol as a reactive surface in the global troposphere, J. Geophys. Res., 101, D17, 22 869–22 889, 1996.
Dey, S., Tripathi, S. N., Singh, R. P., and Holben, B. N.: Influence of dust storms on the aerosol optical properties over the Indo-Gangetic basin, J. Geophys. Res., 109, D20211, doi:10.1029/2004JD004924, 2004.
Dickinson, R., Henderson-Sellers, A., and Kennedy, P.: Biosphereatmosphere transfer scheme (bats) version 1e as coupled to the NCAR community climate model, Technical report, National Center for Atmos. Res., 72 pp., 1993.
Dickerson, R. R., Kondragunta, S., Stenchikov, G., Civerolo, K. L., Doddridge, B. G., and Holben, B.: The impact of aerosols on solar UV radiation and photochemical smog, Science, 278, 827–830, 1997.
Gillette D. A. and Hanson, K. J.: Spatial and temporal variability of dust production caused by wind erosion in the United States, J. Geophys. Res., 94, D2, 2197–2206, 1989.
Ginoux, P. and Torres, O.: Empirical TOMS index for dust aerosol: Applications to model validation and source characterization, J. Geophys. Res., 108, D17, 4534, doi:10.1029/2003JD003470, 2003.
Ginoux, P., Prospero, J., Torres, O., and Chin, M.: Long-term simulation of dust distribution with the GOCART model: Correlation with the North Atlantic Oscillation, Environ. Model. Softw., 19, 113–128, 2004.
Giorgi, F. and Chameides, W. L.: Rainout lifetimes of highly soluble aerosols and gases as inferred from simulations with a general circulation model, J. Geophys. Res., 91, D13, 14 367–14 376, 1986.
Giorgi, F.: Two-dimensional simulations of possible mesoscale effects of nuclear war fires, I: Model description, J. Geophys. Res., 94, D1, 1127–1144, 1989.
Giorgi, F., Marinucci, M., and Bates, G.: Development of a second generation regional climate model (RegCM2), Part I: Boundary layer and radiative transfer processes, Mon. Weather Rev., 121, 2794–2813, 1993a.
Giorgi, F., Marinucci, M., Bates, G., and DeCanio, G.: Development of a second generation regional climate model (RegCM2), Part II: Convective processes and assimilation of lateral boundary conditions, Mon. Weather Rev., 121, 2814–2832, 1993b.
Giorgi, F. and Bi, X. Q.: Direct radiative forcing and regional climatic effects of anthropogenic aerosols over East Asia: A regional coupled climate-chemistry/aerosol model study, J. Geophys. Res., 107, D20, 4439, doi:10.1029/2001JD001066, 2002.

Gong, S. L., Zhang, X. Y., Zhao, T. L., McKendry, I. G., Jaffe, D. A., and Lu, N. M.: Characterization of soil dust aerosol in China and its transport and distribution during 2001 ACE-Asia: 2. Model simulation and validation, J. Geophys. Res., 108, D9, 4262, doi:10.1029/2002JD002633, 2003.

Goudie, A. S.: Dust storms in space and time, Prog. Phys. Geog., 7, 4, 502–530, 1983.

Goudie, A. S. and Middleton, N. J.: The changing frequency of dust storms through time, Climatic Change, 20, 197–225, 1992.

Grousset, F. E., Ginoux, P., Bory, A., and Biscaye, P. E.: Case study of a Chinese dust plume reaching the French Alps, Geophys. Res. Lett., 30, 6, 1277, doi:10.1029/2002GL016833, 2003.

Grell, G. A.: Prognostic evaluation of assumptions used by cumulus parameterizations, Mon. Weather Rev., 121, 764–787, 1993.

Haywood, J. M., Allan, R. P., Culverwell, I., Slingo, T., Milton, S., Edwards, J., and Clerbaux, N.: Can desert dust explain the outgoing longwave radiation anomaly over the Sahara during July 2003?, J. Geophys. Res., 110, D05105, doi:10.1029/2004JD005232, 2005.

Hess, M., Kopke, P., and Schult, I.: Optical properties of aerosols and clouds: The software package OPAC, B. Am. Meteorol. Soc., 79, 831–844, 1998.

Holtslag, A., de Bruijn, E., and Pan, H. L.: A high resolution air mass transformation model for short-range weather forecasting, Mon. Weather Rev., 118, 1561–1575, 1990.

Hou, X. Y.: Vegetation map of China (1:4 000 000), Cartographic Publishing House, Beijing, 1982.

Hsu, S. A.: Thermodynamic characteristics of the subcloud layer affecting haze dispersion along the West coast of Borneo, Pure Appl. Geophys., 160, 419–427, 2003.

Husar, R. B., Tratt, D. M., Schichtel, B. A., Falke, S. R., Li, F., Jaffe, D., Gasso, S., Gill, T., Laulainen, N. S., Lu, F., Reheis, M. C., Chun, Y., Westphal, D., Holben, B. N., Gueymard, C., McKendry, I., Kuring, N., Feldman, G. C., McClain, C., Frouin, R. J., Merrill, J., DuBois, D., Vignola, F., Murayama, T., Nickovic, S., Wilson, W. E., Sassen, K., Sugimoto, N., and Malm, W. C.: Asian dust event of April 1998, J. Geophys. Res., 106, D16, 18 317–18 330, 2001.

Intergovernmental Panel on Climate Change (IPCC), Climate Change 2007: The Physical Science Basis. in: Contribution of WGI to the IPCC AR4. edited by: Solomon, S., Qin, D., Manning, M., Chen, Z., Marquis, M., Averyt, K. B., Tignor, M., Miller, H. L., Cambridge University Press, Cambridge, United Kingdom and New York, NY, USA, 2007.

Joussaume, S.: Three-dimensional simulation of the atmospheric cycle of desert dust particles

using a general circulation model, J. Geophys. Res., 95, D2, 1909–1941, 1990.
Kalnay E., Kanamitsua, M., Kistlera, R., et al.: The NCEP/NCAR 40-Year Reanalysis Project, B. Am. Meteorol. Soc., 77, 437–471, 1996.
Kiehl, J., Hack, J., Bonan, G., Boville, B., Breigleb, B., Williamson, D., and Rasch, P.: Description of the NCAR community climate model (ccm3), Technical report, National Center for Atmos. Res., 152 pp., 1996.
Kurosaki, Y. and Mikami, M.: Recent frequent dust events and their relation to surface wind in East Asia, Geophys. Res. Lett., 30, 14, 1736, doi:10.1029/2003GL017261, 2003.
Liao, H. and Seinfeld, J. H.: Radiative forcing by mineral dust aerosols: sensitivity to key variables, J. Geophys. Res., 103, D24, 31 637–31 646, 1998.
Liu, M., Westphal, D. L., Wang, S., Shimizu, A., Sugimoto, N., Zhou, J., and Chen, Y.: A high-resolution numerical study of the Asian dust storms on April 2001, J. Geophys. Res.,108, D23, 8653, doi:10.1029/2002JD003178, 2003.
Loveland, T. R., Reed, B. C., Brown, J. F., Ohlen, D. O., Zhu, J, Yang, L., and Merchant, J. W.: Development of a Global Land Cover Characteristics Database and IGBP DISCover from 1-km AVHRR Data, Int. J. Remote Sens., 21, 6/7, 1303–1330, 2000.
Luo, C., Mahowald, N., and del Corral, J.: Sensitivity study of meteorological parameters on mineral aerosol mobilization, transport and distribution, J. Geophys. Res., 108, D15, 4447, doi:10.1029/2002JD003483, 2003.
Marticorena, B. and Bergametti, G.: Modeling the atmospheric dust cycle, I, Design of soil-soilderived dust emission scheme, J. Geophys. Res., 100, D8, 16 415–16 430, 1995.
Martin, R. V., Jacob, D. J., Yantosca, R. M., Chin, M., and Ginoux, P.: Global and regional decreases in tropospheric oxidants from photochemical effects of aerosols, J. Geophys. Res., 108, D3, 4097, doi:10.1029/2002JD002622, 2003.
McKendry, I. G., Hacker, J. P., Stull, R., Sakiyama, S., Mignacca, D., and Reid, K.: Long-range transport of Asian dust to the Lower Fraser Valley, British Columbia, Canada, J. Geophys. Res., 106, D16, 18 361–18 370, 2001.
Miller, R. L.: Feedback upon dust emission by dust radiative forcing through the planetary boundary layer, J. Geophys. Res., 109, D24, D24209, doi:10.1029/2004JD004912, 2004.
Myhre, G. and Stordal, F.: Global sensitivity experiments of the radiative forcing due to mineral aerosols, J. Geophys. Res., 106, D16, 18 193–18 204, 2001.
Mitchell, T. D. and Jones., P. D.: An improved method of constructing a database of monthly climate observations and associated high-resolution grids, Int. J. Climatol., 25, 693–712,

2005.
Natsagdorj, L., Jugder, D., and Chung, Y. S.: Analysis of dust storms observed in Mongolia during 1937–1999, Atmos. Environ., 37, 1401–1411, 2003.
Nickovic, S., George, K., Anastasios, P., and Olga, K.: A model for prediction of desert dust cycle in the atmosphere, J. Geophys. Res., 106, D16, 18 113–18 129, 2001.
Pal, J. S., Small, E. E. and Eltahir, E. A. B.: Simulation of regional-scalewater and energy budgets: Representation of subgrid cloud and precipitation processes within RegCM, J. Geophys. Res., 105, D24, 29 579–29 594, 2000.
Pal, J. S., Giorgi, F., Bi, X., Elguindi, N., Solmon, F., Gao, X., Rauscher, S. A., Francisco, R., Zakey, A., Winter, J., Ashfaq, M., Syed, F. S., Bell, J. L., Diffenbaugh, N. S., Karmacharya, J., Konare, A., Martinez, D., da Rocha, R. P., Sloan, L. C., and Steiner, A.: Regional climate modeling for the developing world: The ICTP RegCM3 and RegCNET, B. Am. Meteorol. Soc., 88, 9, 1395–1409, 2007.
Perlwitz, J., Tegen, I., and Miller, R. L.: Interactive soil dust aerosol model in the GISS GCM: 1. Sensitivity of the soil dust cycle to radiative properties of soil dust aerosols, J. Geophys. Res., 106, D16, 18 167–18 192, 2001.
Porter, S. C.: Chinese loess record of monsoon climate during the last glacial-interglacial cycle, Earth Sci. Rev., 54, 115–128, 2001.
Prospero, J. M., Ginoux, P., Torres, O., Nicholson, S. E., and Gill, T. E.: Environmental characterization of global sources of atmospheric soil dust identified with the NIMBUS 7 Total Ozone Mapping Spectrometer (TOMS) absorbing aerosol product, Rev. Geophys., 40, 2–31, 2002.
Pye, K.: Aeolian Dust and Dust Deposits, Academic Press, London, 334 pp., 1987.
Qin, D. H.: Assessment for evolution of environment in Western China, Science Press, Beijing, 2002 (in Chinese).
Rao, S. T., Ku, J. Y., Berman, S., Zhang, K., and Mao, H.: Summertime characteristics of the atmospheric boundary layer and relationships to ozone levels over the Eastern United States, Pure Appl. Geophys., 160, 21–55, 2003.
Shao, Y. and Leslie, L. M.: Wind erosion prediction over the Australian continent, J. Geophys. Res., 102, D25, 30 091–30 105, 1997.
Shao, Y. and Wang, J. J.: A climatology of northeast Asian dust events, Meteorol. Z., 12, 175–183, 2003.
Shao, Y. and Dong, C.: A review on East Asian dust storm climate, modelling and monitoring,

Glob. Planet. Change., 52, 1–22, doi:10.1016/j.gloplacha.2006.02.011, 2006.
Shell, K. M. and Someville, R. C. J.: Direct radiative effect of mineral dust and volcanic aerosols in a simple aerosol climate model, J. Geophys. Res., 112, D03205, doi:10.1029/2006JD007197, 2007.
Sokolik, I. N. and Toon, O. B.: Direct radiative forcing by anthropogenic airborne mineral aerosols, Nature, 381, 681–683, 1996.
Sokolik, I. N., Winker, D. M., Bergametti, G., Gillette, D. A., Carmichael, G., Kaufman, Y. J., Gomes, L., Schuetz, L., and Penner, J. E.: Introduction to special section: outstanding problems in quantifying the radiative impacts of mineral dust, J. Geophys. Res., 106, D16, 18 015–18 027, 2001.
Solmon, F., Giorgi, F., and Liousse, C.: Aerosol modeling for regional climate studies: Application to anthropogenic particles and evaluation over a European/African domain, Tellus B, 58, 1, 51–72, 2006.
Tanaka, T. Y., Orito, K., Sekiyama, T. T., Shibata, K., Chiba, M., and Tanaka, H.: MASINGAR, a global tropospheric aerosol chemical transport model coupled with MRI/JMA98 GCM: model description, Pap. Meteorol. Geophys., 53, 119–138, 2003.
Tegen, I. and Fung, I.: Modeling of mineral dust in the atmosphere: sources, transport, and optical thickness, J. Geophys. Res., 99, D11, 22 897–22 914, 1994.
Tegen, I. and Lacis, A. A.: Modeling of particle size distribution and its influence on the radiative properties of mineral dust aerosol, J. Geophys. Res., 101, D14, 19 237–19 244, 1996.
Tegen, I., Harrison, S. P., Kohfeld, K., Prentice, I. C., Coe, M., and Heimann, M.: Impact of vegetation and preferential source areas on global dust aerosol: results from a model study, J. Geophys. Res., 107, D21, 4576, doi:10.1029/2001JD000963, 2002.
USDA: Soil Taxonomy, a basic system of Soil Classification for making and interpreting Soil Surveys, US Government Printing Office, Washington, 869 pp., 1999.
Westphal, D. L., Toon, O. B., and Carson, T. N.: A case study of mobilisation and transport of Saharan dust, J. Atmos. Sci., 45, 2145–2175, 1988.
Woodward, S.: Modeling the atmospheric lifecycle and radiative impact of mineral dust in the Hadley Centre climate model, J. Geophys. Res., 106, D16, 18 155–18 166, 2001.
Yoshioka, M., Mahowald, N. M., Conley, A. J., Collins, W. D., Fillmore, D. W., Zender, C. S., and Coleman, D. B.: Impact of desert dust radiative forcing on Sahel precipitation: relative importance of dust compared to sea surface temperature variations, vegetation changes, and greenhouse gas warming, J. Climate, 20, 1445–1467, 2007.

Zakey, A. S., Solmon, F., and Giorgi, F.: Implementation and testing of a desert dust module in a regional climate model, Atmos. Chem. Phys., 6, 4687–4704, 2006

Zender, C. S., Bian, H., and Newman, D.: Mineral Dust Entrainment and Deposition (DEAD) model: description and 1990s dust climatology, J. Geophys. Res., 108, D14, 4416, doi:10.1029/2002JD002775, 2003.

Zender, C. S., Miller, R. L., and Tegen, I.: Quantifying mineral dust mass budgets: Terminology, constraints, and current estimates, Eos Trans. Am. Geophys. Union, 85, 48, 509–512, 2004.

Zhang, D. E.: Synoptic–climatic studies of dust fall in China since historic times, Sci. Sinica., Ser. B, Chem. Biol. Agric. Med. Earth Sci., 27, 825–836, 1984.

Zhang, D. F., Ouyang, L. C., Gao, X. J., Giorgi, F., and Pal, J. S.: Simulation of the atomospheric circulation over East Asia and climate in China by RegCM3, J. Tropical Meteor., 23, 5, 444–452, 2007 (in Chinese).

Zhang, J. and Christopher, S. A.: Longwave radiative forcing of Saharan dust aerosols estimated from MODIS, MISR, and CERES observation on Terra, Geophys. Res. Lett., 30, 23, 2188, doi:10.1029/2003GL018479, 2003.

Zhang, R. J., Han, Z. W., Wang, M. X., and Zhang, X. Y.: Dust storm weather in China: new characteristics and origins, Quat. Sci., 22, 4, 374–380, 2002 (in Chinese).

Zhang, X. Y.: Source distributions, emission, transport, deposition of Asian dust and Loess accumulation, Quat. Sci., 21, 29–38, 2001.

Zhang, X. Y., Gong, S. L., Zhao, T. L., Arimoto, R., Wang, Y. Q., and Zhou, Z. J.: Sources of Asian dust and role of climate change versus desertification in Asian dust emission, Geophys. Res. Lett., 30, 24, 2272, doi:10.1029/2003GL018206, 2003a.

Zhang, X. Y., Gong, S. L., Arimoto, R., Shen, Z. X., Mei, F. M., Wang, D., and Cheng, Y.: Characterization and temporal variation of Asian dust aerosol from a site in the northern Chinese deserts, J. Atmos. Chem., 44, 241–257, 2003b.

Zhao, C. S., Tie, X. X., and Lin, Y. P.: A possible positive feedback of reduction of precipitation and increase in aerosols over eastern China, Geophys. Res. Lett., 33, L11814, doi:10.1029/2006GL025959, 2006a.

Zhao, L. N. and Zhao, S. X.: Diagnosis and simulation of a rapidly developing cyclone related to a severe dust storm in East Asia, Global Planet. Change, 52, 105–120, doi:10.1016/j.gloplacha.2006.02.003, 2006b.

Zhou, Z. J.: Blowing sand and sand storm in China in recent 45 years, Quat. Sci., 21, 9–17, 2001.

Zhou, Z. J. and Zhang, G. C.: Typical severe dust storms in northern China during 1954–2002, Chinese Sci. Bull., 48, 21, 2366–2370, 2003.

Table 1. Distribution of dust source regions.

Name	Lat (°N)	Lon (°E)	Area (km^2)
Taklimakan	39.0	83.0	337 600
Gurbantunggut	45.1	87.3	48 800
Kumtag	39.7	92.0	22 900
Badain Jaran	40.4	102.0	44 300
Tengger	38.0	104.2	42 700
Ulan Buh	40.4	106.5	9900
Hobq	40.5	107.9	16 100
Mu Us	38.8	109.1	32 100
Onqin Daga	43.0	115.0	21 400
Horqin	43.3	122.0	42 300

ACPD
8, 4625–4667, 2008

Table 2. Information for the selected nine stations.

Name	Lat (°N)	Lon (°E)	Height (m)
Ulmuqi	43.43	87.38	918.7
Lanzhou	36.52	103.62	1518.3
Yinchuan	38.37	106.37	1112.7
Huhhot	40.49	111.37	1065.0
Taiyuan	37.80	112.30	776.6
Shijiazhuang	38.05	114.48	81.2
Beijing	39.56	116.17	32.0
Qingdao	36.04	120.22	77.2
Shanghai	31.24	121.28	8.2

Table 3. Correlation coefficient between TOMS AI and modeled DI in FMAM.

	1997	1998	1999	2000	2001	2002	2003	2004	2005	2006	ave
West	0.08	0.48	0.21	0.62	0.27	0.48	0.33	0.48	0.47	0.32	0.35
Central	−0.21	0.53	0.18	0.39	0.50	0.21	0.19	−0.03	0.17	0.43	0.27
East	0.02	0.55	0.25	0.62	0.53	0.52	0.40	0.23	0.53	0.51	0.41

ACPD
8, 4625–4667, 2008

Table 4. Percentage of occurrence of dust storm events (emission thresholds of 5000/10 000/15 000 mg m^{-2} day^{-1}).

	February	March	April	May
West	8/7/4	27/28/30	31/40/46	34/25/20
Central	17/19/20	31/34/38	30/33/33	22/15/9
East	5/7/10	22/16/30	47/61/50	26/16/10
W+C+E	11/13/14	28/30/34	33/38/39	28/19/13

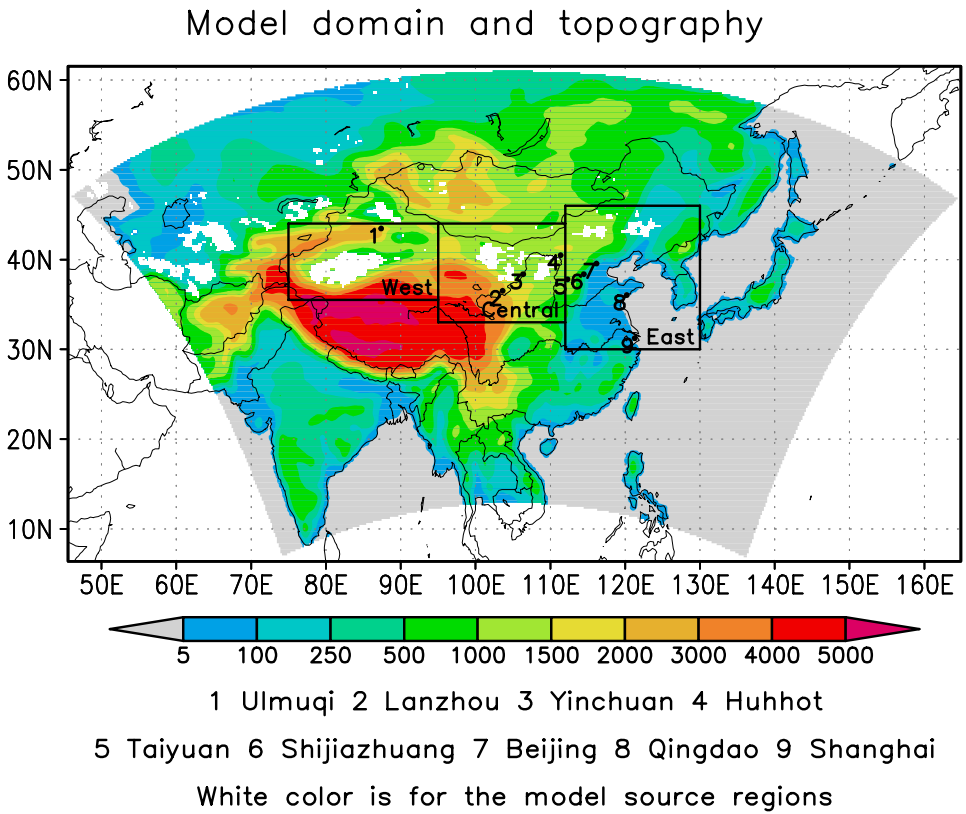

Fig. 1. Model domain and topography. Units are meters. Also shown are the three regions and the location of nine stations selected for the study.

ACPD
8, 4625–4667, 2008

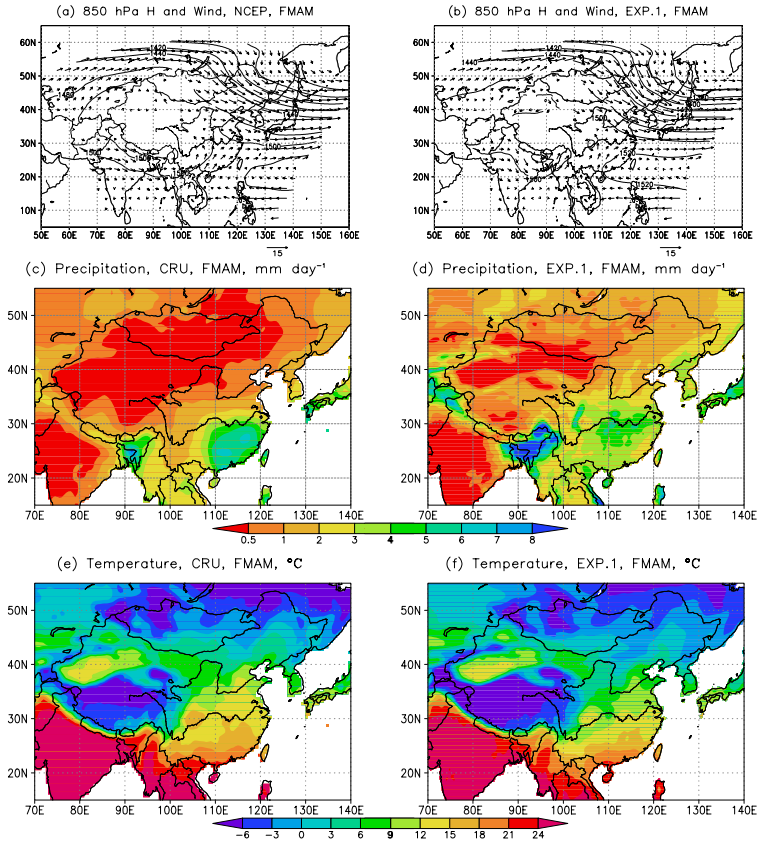

Fig. 2. Mean (1997–2006) 850 hPa height (contour line) and wind (arrows) in FMAM from NCEP reanalysis **(a)** and model simulation **(b)**; observed (**c**, 1997–2002, available data), and simulated (**d**, 1997–2006) mean precipitation; observed (**e**, 1997–2002, available data), and simulated (**f**, 1997–2006) mean temperature. Units are meters for height, m s^{-1} for wind, mm day^{-1} for precipitation, °C for temperature.

ACPD
8, 4625–4667, 2008

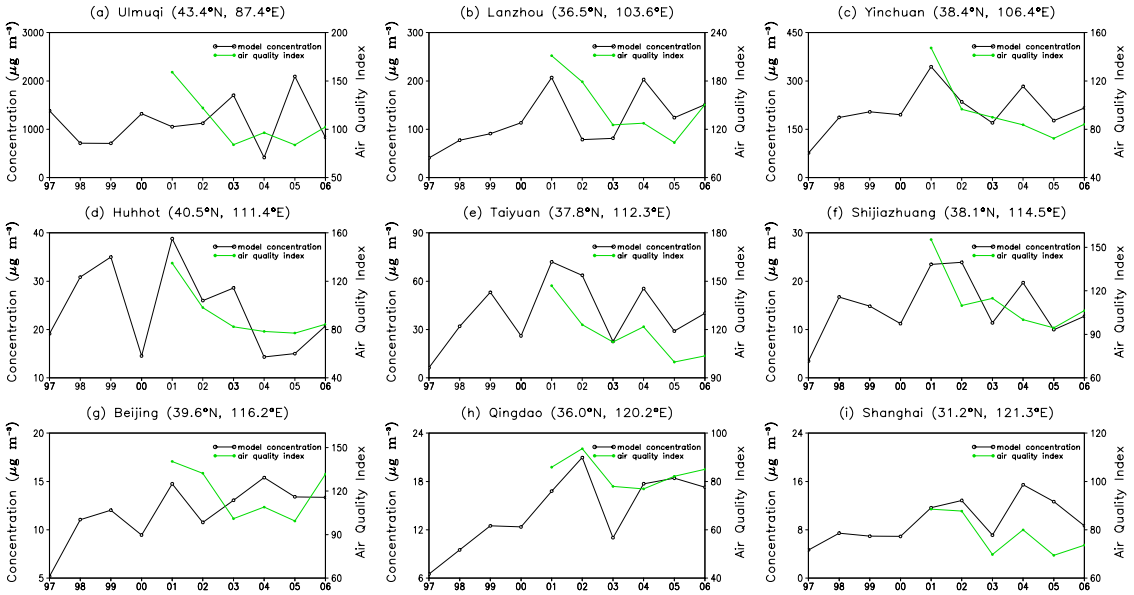

Fig. 3. Observed mean air quality index (2001–2006, available data) and simulated near surface dust concentration (1997–2006) in FMAM at the nine stations. Units are $\mu g\,m^{-3}$ for concentration.

ACPD
8, 4625–4667, 2008

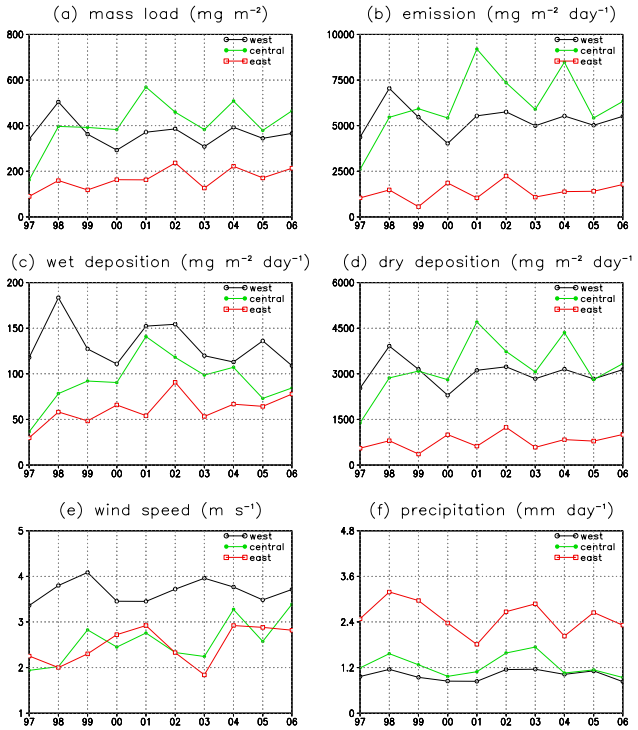

Fig. 4. Simulated annual mean **(a)** mass load, **(b)** emission, **(c)** wet deposition, **(d)** dry deposition, **(e)** wind speed, **(f)** precipitation for the three regions (see Fig. 1). Units are mg m^{-2} for mass load, mg m^{-2} day^{-1} for emission, wet and dry deposition, m s^{-1} for wind, mm day^{-1} for precipitation.

ACPD
8, 4625–4667, 2008

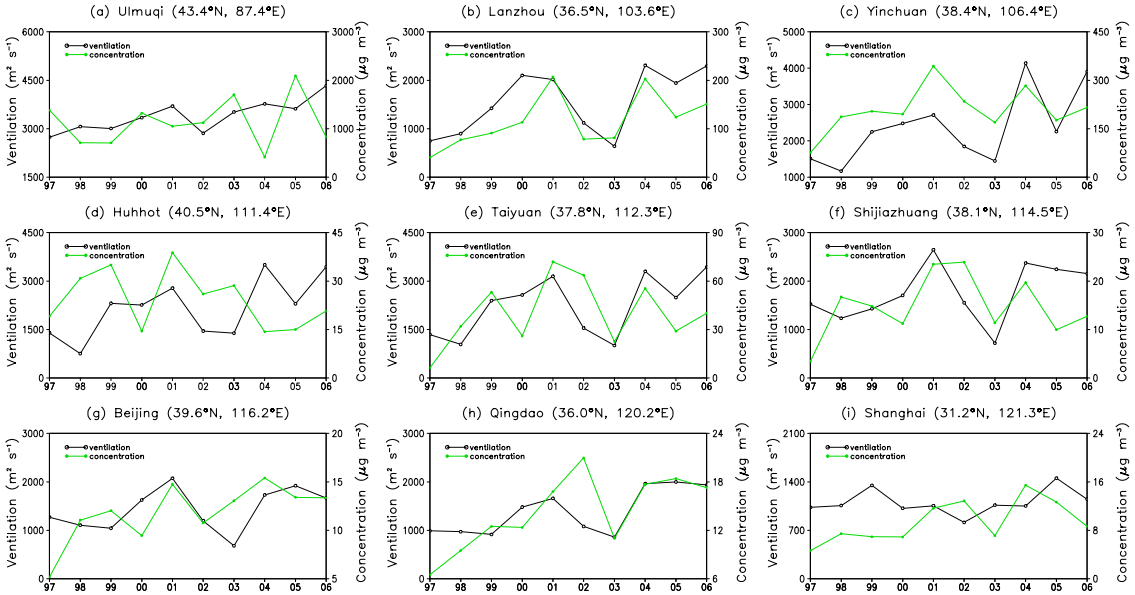

Fig. 5. Simulated annual mean ventilation index and concentration at the nine stations. Units are $\mu g\,m^{-3}$ for concentration and $m^2\ s^{-1}$ for the ventilation index.

ACPD
8, 4625–4667, 2008

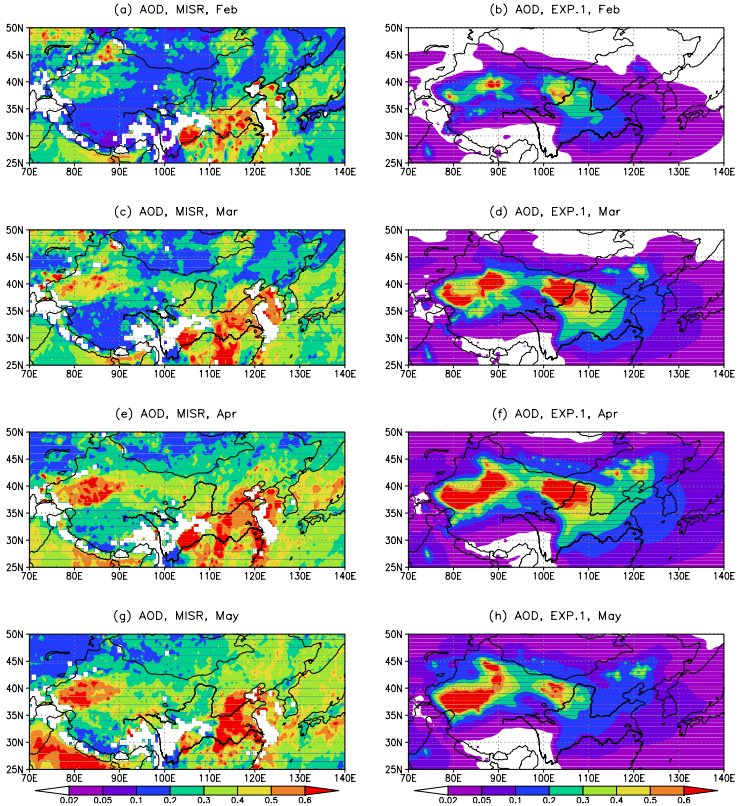

Fig. 6. Observed monthly mean AOD from MISR observations (550 nm) (2001–2006, available data) in **(a)** February, **(c)** March, **(e)** April, **(g)** May and from the model simulation (1997–2006) in **(b)** February, **(d)** March, **(f)** April, **(h)** May.

ACPD
8, 4625–4667, 2008

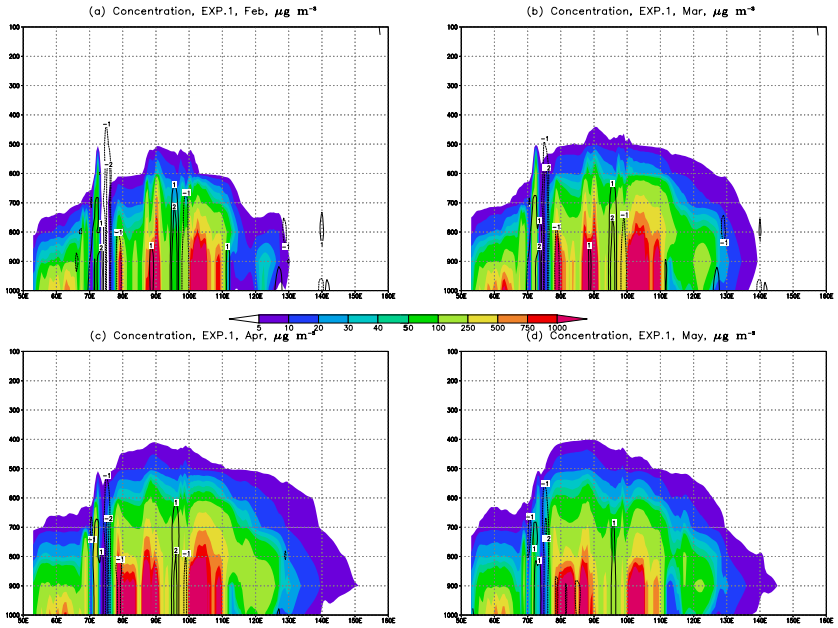

Fig. 7. Simulated longitude-height cross section of dust concentration (shaded) and divergence (contour line) averaged over 1997–2006. **(a)** February, **(b)** March, **(c)** April, **(d)** May. Units are μg m^{-3} for concentration and s^{-1} *e5 for divergence.

ACPD
8, 4625–4667, 2008

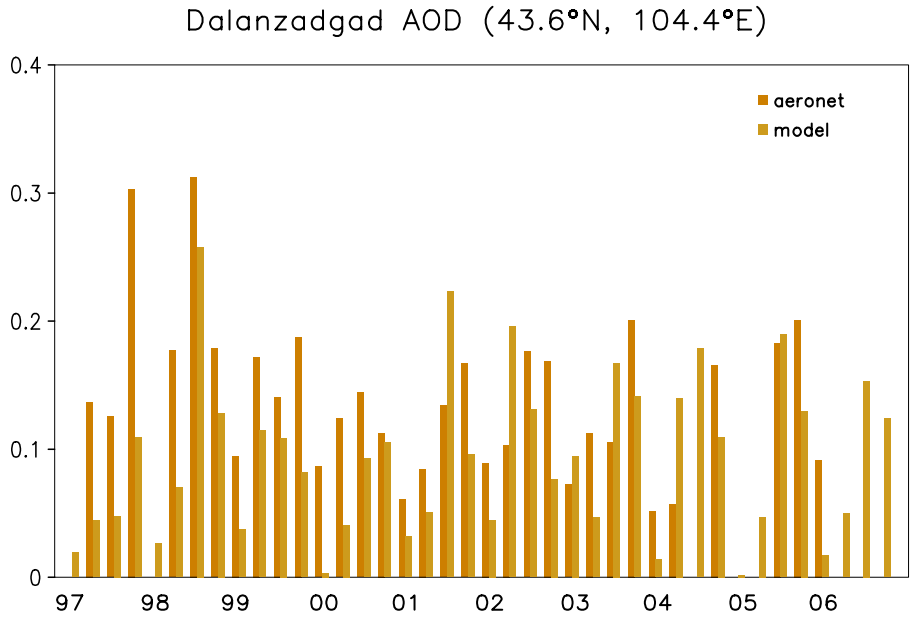

Fig. 8. Monthly mean aerosol optical depth from AERONET observations (500 nm) and from the model simulation (550 nm) at Dalanzadgad.

ACPD
8, 4625–4667, 2008

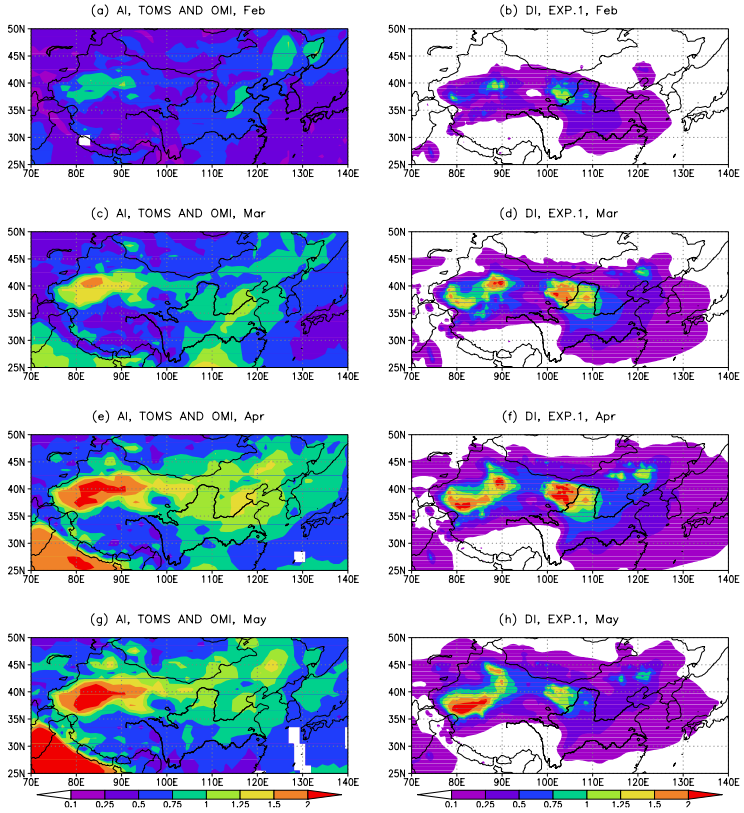

Fig. 9. Observed monthly mean AI from TOMS (1997–2005, available data) and OMI (2006) in **(a)** February, **(c)** March, **(e)** April, **(g)** May; and simulated DI (1997–2006) in **(b)** February, **(d)** March, **(f)** April, **(h)** May.

ACPD
8, 4625–4667, 2008

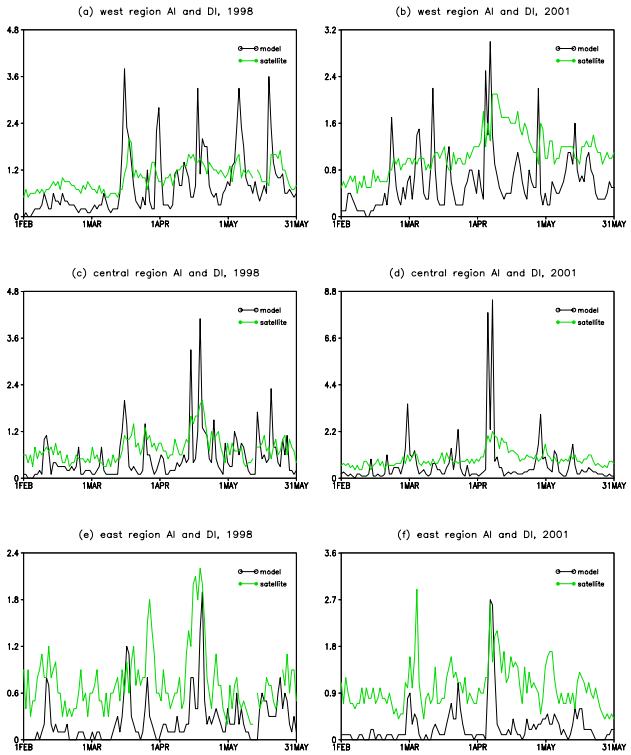

Fig. 10. Daily AI from TOMS and DI from simulation from February through May over the three regions in 1998 **(a, c, e)** and 2001 **(b, d, f)**.

ACPD
8, 4625–4667, 2008

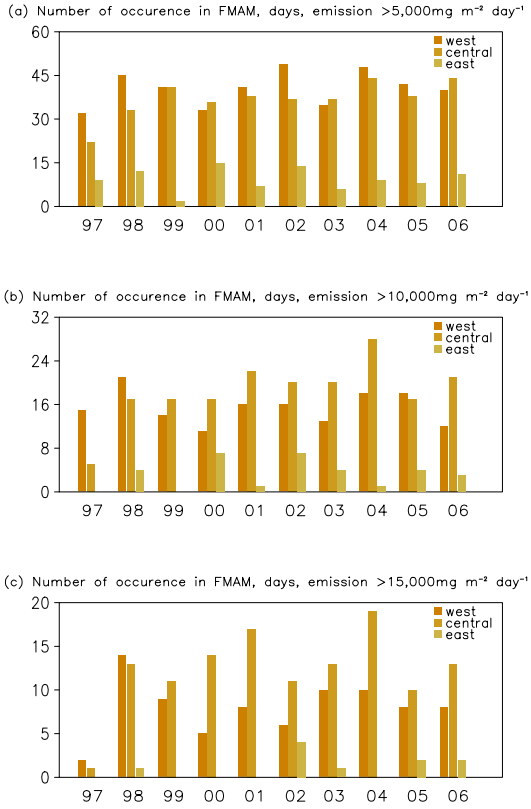

Fig. 11. Number of the occurrence of dust events in the three regions of West, Central and East in FMAM from 1997 to 2006, as defined by the emission thresholds 5000 **(a)**, 10 000 **(b)** and 15 000 mg $m^{-2}day^{-1}$ **(c)**. Units are number of days.

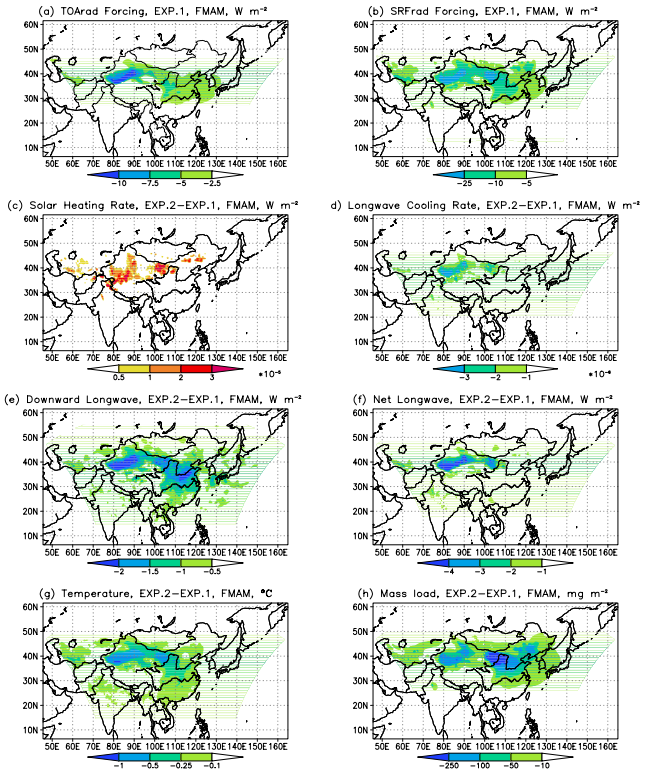

Fig. 12. Dust feedback effects. **(a)** dust TOA radiative forcing, **(b)** dust surface radiative forcing, **(c)** difference of solar heating rate (W m^{-2}) between Exp. 1 and Exp. 2, **(d)** difference of long-wave cooling rate (W m^{-2}) between Exp. 1 and Exp. 2, **(e)** difference of downward long-wave solar radiation (W m^{-2}) between Exp. 1 and Exp. 2, **(f)** difference of net long-wave solar radiation (W m^{-2}) between Exp. 1 and Exp. 2, **(g)** difference of surface air temperature between Exp. 1 and Exp. 2, **(h)** difference of dust mass load (mg m^{-2}) between Exp. 1 and Exp. 2.

ACPD
8, 4625–4667, 2008

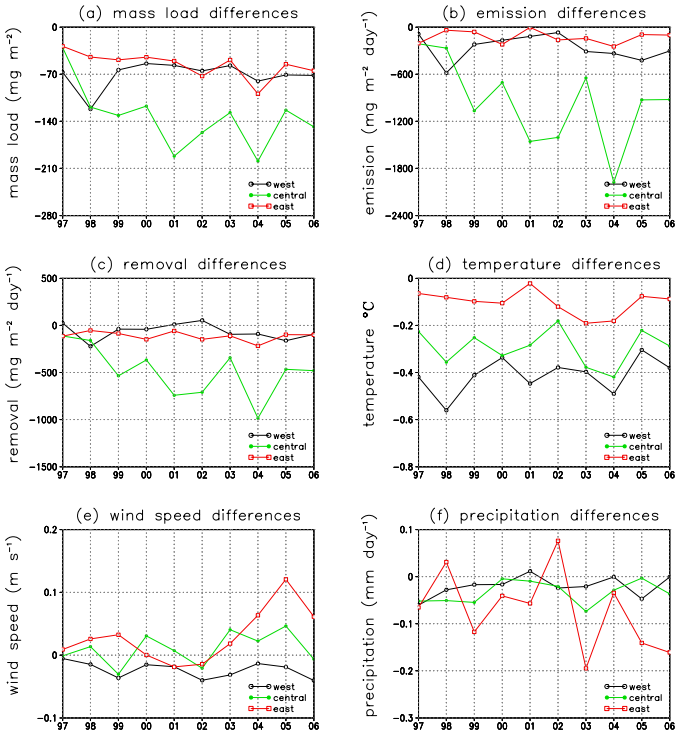

Fig. 13. Differences between Exp. 1 and Exp. 2 over the three regions of **(a)** mass load (mg m^{-2}), **(b)** dust emission (mg m^{-2} day^{-1}), **(c)** dust removal (mg m^{-2} day^{-1}), **(d)** surface air temperature (°C), **(e)** wind speed (m s^{-1}), and **(f)** precipitation (mm day^{-1}).

ACPD
8, 4625–4667, 2008